Katholieke Universiteit Leuven

Departement Elektrotechniek ESAT-SISTA/TR 06-35

Fast Nosologic Imaging of the brain [1]

Maarten De Vos, Teresa Laudadio, Arjan Simonetti, Arend Heerschap, Sabine Van Huffel[2]

March 2006
Internal Report

[1]This report is available by anonymous ftp from *ftp.esat.kuleuven.ac.be* in the directory *pub/sista/mdevos/reports/KVIV2006.ps.gz*

[2]K.U.Leuven, Dept. of Electrical Engineering (ESAT), Research group SISTA, Kardinaal Mercierlaan 94, 3001 Leuven, Belgium, Tel. 32/16/32 17 09, Fax 32/16/32 19 70, WWW: *http://www.esat.kuleuven.ac.be/sista*. E-mail: *maarten.devos@esat.kuleuven.be*. Research funded by a PhD grant of the Institute for the Promotion of Innovation through Science and Technology in Flanders (IWT-Vlaanderen).

Fast nosologic imaging of the brain

M. De Vos∗, T. Laudadio∗, A.W. Simonetti∗, A. Heerschap† and S. Van Huffel∗
∗ *Katholieke Universiteit Leuven, Department of Electrical Engineering, Division ESAT–SCD (SISTA), Kasteelpark Arenberg 10, 3001 Leuven-Heverlee, Belgium;*
† *University of Nijmegen, University Medical Center St. Radboud, Department of Radiology, Geert Grooteplein Z18, PO Box 9101, 6500 HB Nijmegen, The Netherlands*

Version: March 6, 2006

Magnetic Resonance Spectroscopic Imaging (MRSI) is able to provide information about the spatial metabolic heterogeneity of an organ in the body. In this way, MRSI can be used to detect regions with abnormal tissue metabolism, e.g. tumor tissue. The main drawback in clinical practice is that the analysis of MRSI data requires a lot of expertise from the radiologists. In this article we present an automatic method that assigns each voxel of a spectroscopic image of the brain to a histopathological class. The method is based on Canonical Correlation Analysis (CCA), which has recently been shown to be a robust technique for tissue typing. In this paper, we introduce a new CCA-based method in which we integrate MRSI and MR imaging information. We compare the performance of the CCA-based methods obtained by applying CCA to the whole MR spectra and to sets of features, respectively. Tests on simulated and *in vivo* MRSI data show that the new method is very accurate in terms of classification and segmentation. The results also show the advantage of combining spectroscopic and imaging data.

Key Words: Magnetic Resonance Spectroscopic Imaging, Magnetic Resonance Imaging, Tissue Segmentation, Canonical Correlation Analysis, Classification, Brain Tumors

1. INTRODUCTION

Magnetic resonance spectroscopy (MRS) is increasingly be used in the diagnosis of brain tumors, for choosing the most appropriate therapy and for therapy follow-up. With single voxel proton MRS, tissue concentrations of metabolites can be determined in a well-defined voxel of the organism under investigation in a non-invasive way. This can reduce the need for a biopsy, which is not without risks for the patient *(7)*. However, analysis of MR spectra still requires a lot of expertise from the radiologist. To reduce the need of human interaction, several classifiers have already been proposed that try to distinguish different types of tumor in an automatic way, e.g. *(11, 12, 18, 19, 34, 35)*. Although single voxel proton MRS is a relatively fast method to characterise the metabolic signature of the tumor, radiologists are also interested in its shape, size and (metabolic) heterogeneity. This information can be obtained with multivoxel proton MRSI, in combination with high-quality anatomical MR images *(8)*. During an MRSI examination, metabolic information is measured in a grid of voxels rather than in one voxel. This allows radiologists to extract histopathological information from each voxel as well as information about the heterogeneity of the tumor. However, due to the large amount of data that is acquired and needs to be processed during the investigation of a patient, there is an even stronger need for automatic 'classification' strategies than for single voxel MRS. More correctly, one should speak of 'segmentation' strategies as the goal is to segment an MRS image into regions of different tissues. We will explain how the proposed segmentation method is also able to label the detected segments simultaneously. A variety of methods is available in the literature, and in particular pattern recognition methods are commonly used to segment MRSI data *(12, 30)*. The result of a segmentation is a nosologic image *(38)*. Such an image summarizes the available information by coloring each pixel according to the determined histopathological class. In this way, nosologic images can be routinely and easily used by radiologists for tumor diagnosis.

In this paper we investigate the accuracy and robustness of a Canonical Correlation Analysis (CCA) based method to segment short echo-time brain MRSI data. The main advantage of CCA is the possibility to exploit both spatial and spectral information during the analysis of the spectrum in a voxel. Since it can be expected that the chance to have a normal voxel is much higher when the surrounding voxels are normal as well, including spatial information can improve robustness. Maximal spectral information is also incorporated by generating a representative model spectrum for each tissue class that allows for realistic variations. Recently, CCA has been shown to be a fast and robust method for automated segmentation of long echo-time prostate MRSI data *(21)*. In *(4)*, the same CCA-based method is used to segment long echo-time brain MRSI data of patients with one known tumor type, glioblastoma.

In this paper, we extend this study in various ways. First of all, we focus on short echo-time spectra of the brain. We use short echo-time spectra, because they are more relevant than long echo-time spectra for tumor classification and grading due to the presence of signals of more metabolites, including myo-inositol, glutamate and glutamine *(9, 10, 14, 15, 35)*. However, interpretation of such spectra is complicated by the presence of a broad baseline, originating from macromolecules and lipids *(24, 27, 28)*. The lipid signals may be relevant as indicator of grade *(17, 20)*, but the shape of the macromolecular baseline is in general unpredictable, especially in pathological cases.
Second, for brain tumor diagnosis, it is not sufficient to segment an MRSI image in normal and tumor tissue. Several types and grades of brain tumors may exist in different patients. For choosing the most appropriate therapy, it is very important to distinguish between different grades. In order to deal with different tumor types, we introduce a two-steps CCA approach. We will explain how the first step is a tumor typing step, and how in the second step a segmentation is obtained.
Third, we also show how to combine multimodal information and investigate the influence of adding MRI information to the MRSI data. Four MR images with different contrasts (see §3) were acquired for every patient. This extra information is shown to improve the classification performance in other pattern recognition studies *(38, 30)*. As we will explain below, to integrate MRSI and MRI information in a CCA-based method, a dimension reduction has to be performed on the MR spectra by the extraction of characteristic features. Most other classifiers or pattern recognition methods also use features as input variables, because they cannot deal with high-dimensional input spaces. As the CCA-method can be applied either to a spectrum or to a set of features, it is very interesting to compare the results obtained with both CCA-approaches.

In this paper, we start with a short overview of the theory of CCA and how the method is applied to nosologic imaging of the brain in §2. In §3 we describe how we construct our simulations. Further, we investigate the accuracy of the method on the real part of baseline-corrected spectra. We also compare these results with the results of the CCA-method on features, without and with MRI information. The results on simulated and *in vivo* MRSI are discussed in §4 and §5 respectively. Finally, we formulate our main conclusions in §6. In the appendix, a note on normalisation is added.

2. METHOD

2.1. Canonical Correlation Analysis (CCA)

We shortly describe the mathematical idea of CCA *(13)*. For more details, we refer to *(29)*. A reliable implementation is described in *(21)*. Ordinary correlation analysis quantifies the relation between two variables x and y by means of a correlation coefficient ρ:

$$\rho = \frac{Cov[x,y]}{\sqrt{V[x]V[y]}}$$

CCA is a multivariate extension of ordinary correlation analysis. Consider 2 multivariate zero-mean vectors $\mathbf{x}=[x_1(f),\ldots,x_m(f)]^T$ and $\mathbf{y}=[y_1(f),\ldots,y_n(f)]^T$, $f = 1,..,N$. Two new scalar variables, X and Y, are generated as a linear combination of the components in $\mathbf{x}$ and $\mathbf{y}$:

$$\begin{aligned} X &= w_{x_1}x_1 + \ldots + w_{x_m}x_m = \mathbf{w}_x^T\mathbf{x} \\ Y &= w_{y_1}y_1 + \ldots + w_{y_m}y_m = \mathbf{w}_y^T\mathbf{y} \end{aligned}$$

CCA computes the coefficients $\mathbf{w}_x$ and $\mathbf{w}_y$ that maximize the correlation between X and Y. These coefficients are called regression weights and X and Y are called canonical variates. The resulting correlation coefficient is called the canonical correlation coefficient.

2.2. Applying CCA to spectra

During an MRSI acquisition, MR spectra are measured in a grid of voxels. Based on the information contained in these spectra, we want to segment our image in different regions. All the voxels in one region belong to the same tissue type. Each voxel can be assigned individually to a certain tissue type by using a sophisticated single voxel classifier like LS-SVM *(34)* or simply by computing the correlation or distance between the spectrum in the considered voxel and a known tissue type model *(38)*. However, with this approach, the spatial information provided by multivoxel MRS is not used. When all the surrounding voxels contain healthy tissue, the considered voxel also has a very high probability to contain healthy tissue. CCA exploits this spatial information by considering a multivariate vector $\mathbf{X}$ that contains the spectrum of the voxel under investigation and some spectra of the surrounding voxels. Several spatial models can be used. In this study, we compare the results obtained with the following spatial models:

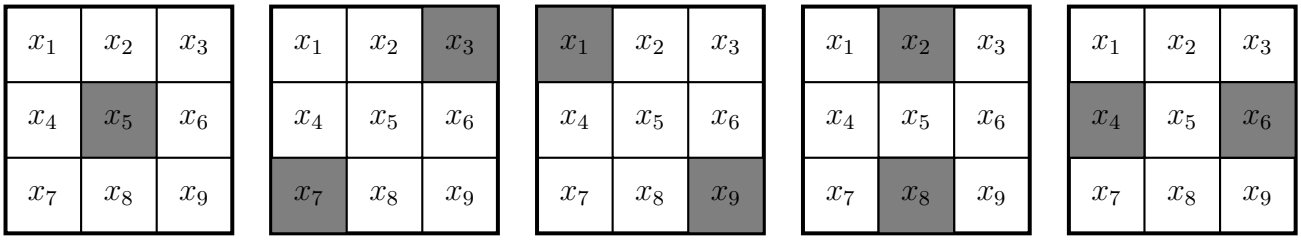

FIG. 1: The components of a spatial model of CCA, called the 'symmetric 3x3'

- the 'symmetric 3x3' model (figure 1):

$$\mathbf{X} = \begin{pmatrix} x_5(f) \\ \frac{x_1(f)+x_9(f)}{2} \\ \frac{x_2(f)+x_8(f)}{2} \\ \frac{x_3(f)+x_7(f)}{2} \\ \frac{x_4(f)+x_6(f)}{2} \end{pmatrix}$$

- the '3x3' model:

$$\mathbf{X} = \begin{pmatrix} x_5(f) \\ x_1(f) \\ x_2(f) \\ x_3(f) \\ x_4(f) \\ x_6(f) \\ x_7(f) \\ x_8(f) \\ x_9(f) \end{pmatrix}$$

- the '3x3 without corners' model:

$$\mathbf{X} = \begin{pmatrix} x_5(f) \\ x_2(f) \\ x_4(f) \\ x_6(f) \\ x_8(f) \end{pmatrix}$$

- the 'symmetric 3x3 without corners' model:

$$\mathbf{X} = \begin{pmatrix} x_5(f) \\ \frac{x_2(f)+x_8(f)}{2} \\ \frac{x_4(f)+x_6(f)}{2} \end{pmatrix}$$

- the 'star' model:

$$\mathbf{X} = \begin{pmatrix} x_5(f) \\ \frac{x_5(f)+x_2(f)}{2} \\ \frac{x_5(f)+x_4(f)}{2} \\ \frac{x_5(f)+x_6(f)}{2} \\ \frac{x_5(f)+x_8(f)}{2} \end{pmatrix}$$

In the case of the spatial 'star' model, it can be seen that the information contained in the voxel under investigation (x_5) is always used at least as much as the information in the surrounding voxels. For the voxels at the borders of the image, it is not possible to construct these spatial models. In order to overcome this problem, two additional rows and two additional columns are generated by copying the first and last rows and columns of the original grid.
During the classification of a voxel, CCA also integrates as much spectral information as possible in a spectral model, the multivariate $\mathbf{Y}$. The first component y_1 of this spectral model for each tissue type is constructed as the mean of a database containing *in vivo* spectra, characteristic of that tissue type. To model natural inter-spectral and inter-patient variability, a variational component y_2 is computed as follows. First the computed mean is subtracted from all *in vivo* spectra in the database. Secondly, PCA is performed on this mean-subtracted database. The first principal component contains most of the variations, and is used as y_2.

To obtain a segmentation with CCA, canonical correlation coefficients are computed with the chosen spatial model and the spectral models of different tissue types. A visual representation of the analysis of one voxel (x_5) with a certain tissue type is given in figure 2. The computed canonical correlation coefficients indicate how likely it is that the considered voxel belongs to the different tissue types. In the case of three tissue types, these three canonical correlation coefficients can be displayed in the 3-dimensional coordinate system (first canonical correlation coefficient, second canonical correlation coefficient and third canonical correlation coefficient). The distribution of the voxels in this coordinate system is displayed for a simulated MRS image with normal, mixed and tumor tissue in figure 3. Three clouds of points can be distinguished, corresponding to the three present tissue types. The blue voxels have a high correlation with normal tissue, the red voxels have a high correlation with tumor tissue and the green voxels lie between both clouds. A clustering method *(36)* can be applied to these canonical correlation coefficients. However, in order to avoid well-known problems of clustering algorithms (e.g. initialisation, number of clus-

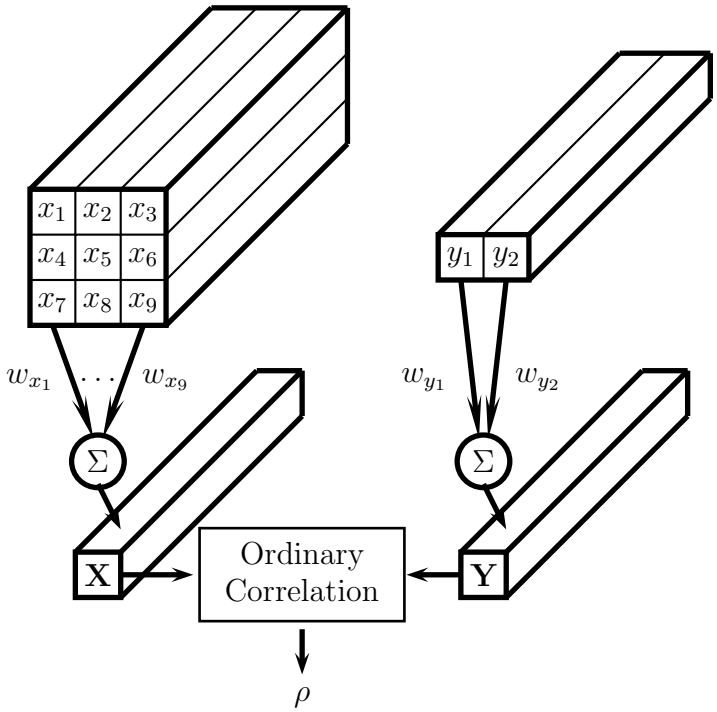

FIG. 2: Diagram of applying CCA to MRSI. We want to assign voxel x_5 to a tissue type. The other x_i are surrounding voxels that will also be used in the analysis of voxel x_5. y_1 is the model spectrum of a certain tissue, and y_2 takes into account realistic variations. CCA computes the regression weights w_{x_i} and w_{y_i} in order to maximize the correlation between X and Y

ters, . . .), another criterion is used to assign a voxel to a certain tissue type: the highest canonical correlation coefficient.

2.3. A two-steps CCA-based method

As there exist several grades of brain tumor malignancy, a model spectrum has to be constructed for all tumor types and for all corresponding mixed tissues. It can be expected that only one tumor type is present in a patient.
CCA is able to discriminate between different tumor types, but we noticed that voxels with mixed tissue are not always correctly detected. To avoid this problem a two-steps method is proposed. The first step is a tumor typing step and the second the segmentation step. In the first step only the model spectra of normal tissue, CSF and the different tumor spectra are used. As CCA is able to discriminate between all grades, this step is only to detect the present type of tumor. In the second step, CCA is applied with the model spectrum from CSF, normal tissue, the detected tumor tissue and corresponding mixed tissue. In this step, the heterogeneity of the tumor is shown.

2.4. Feature-based approach

When we want to integrate the available MRSI and MRI information in the CCA-based method, harmonisation of both input spaces is necessary. This multimodal integration requires 2 steps, which we now describe.
At most 4 images with different contrasts are acquired during a study. These 4 extra variables per voxel won't influence the result, when we just add these 4 variables to the spectra (of 1024 datapoints) due to the large difference in number of datapoints. We firstly have to summarize the spectra into representative features. This dimension reduction can be done by applying PCA or quantifying the spectra. The second way is most meaningful, since the quantified amplitudes are a direct estimate of the concentrations of the most important metabolites. Several quantification methods for short echo time spectra can be used. Amares is namely conceived for long echo-time MRS data quantification *(23)* and requires too much user interaction in the quantification of short echo-time MRS data *(5)*. At this moment there exist three easy-to-use quantitation tools: the commercially available LCModel *(41)*,

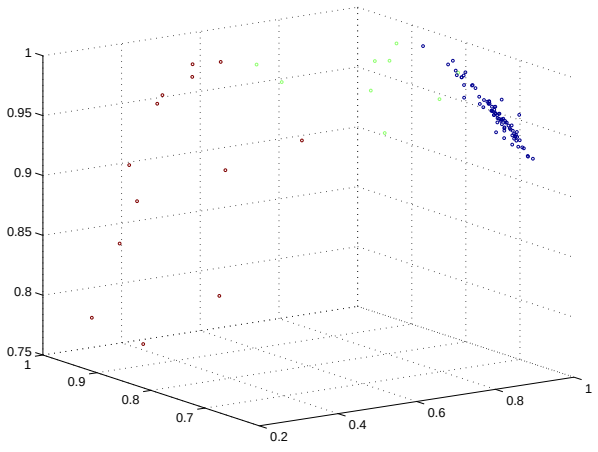

FIG. 3: All voxels in a MRSI grid are displayed in the coordinate system of the computed canonical correlation coefficients with different tissue types. Three clouds corresponding to the three present tissue types are visible

the freely available QUEST *(33)* and the recently introduced open-source package AQSES *(42)*. For the present study we used AQSES, that fits an *in vivo* spectrum in the complex time domain as a linear combination of *in vitro* metabolite spectra. To avoid overfitting, only the 8 most important metabolites (Myo-inositol, Choline, Creatine, Glutamine, Glutamate, NAA, Alanine and Lactate) were quantified, together with the lipid peaks at 0.9 and 1.3 ppm. These metabolite levels formed the first 10 values in the set of features.

In addition to feature reduction, also the spatial resolution of both imaging modalities has to be matched. This can be done in several ways: lowering the resolution of the MR image to MRSI voxel size, keeping the MRI resolution and interpolating between MRSI voxels, or a combination of both. A detailed comparison of the best way to integrate both modalities is beyond the scope of this paper. We decided to lower the resolution of the MR image to MRSI voxel size.

So, the images with 4 contrasts were aligned with respect to the spectroscopic image and the MR pixel intensities were averaged out over a spectroscopic voxel. These MRI variables were scaled to be in the same range as the quantified metabolite concentrations. These 4 image variables formed the last 4 values in the set of features.

Although the application of the CCA method either on spectra or on features doesn't differ, the implementation does. The aim of the spatial model of CCA is to reduce the noise by 'averaging out' some voxels. In order to obtain a realistic solution, all the regression weights of X should have the same sign. When the CCA-method is applied to spectra, the mathematically optimal solution satisfies most of the time this constraint. However, in the feature case, this constraint is violated with the implementation given in *(21)*, and has to be imposed explicitly. In *(3, 6)* it is proven that an elegant constrained CCA solution exists in the special case the regression weights are imposed to be non-negative. Such a constrained CCA solution equals an *unconstrained* CCA solution when one or several variables have been excluded. Formally, consider the sequence $\mathbb{N}_k = \{1, 2, \ldots, k\}$ where k is a positive integer and all its possible subsequences $\mathbb{W}_k = \{\mathbf{a} | \mathbf{a} \subseteq \mathbb{N}_k\}$. When $\mathbf{x}$ is a m-dimensional vector and $\mathbf{a} \in \mathbb{W}_m$, ${}_{\mathbf{a}}\mathbf{x}$ denotes the vector obtained when only the components listed in $\mathbf{a}$ are kept. If we denote with $\rho(\mathbf{x}, \mathbf{y})$ the canical correlation coefficient between x and y, then the solution ρ of the constrained CCA problem is found in the following set:

$$\bigcup_{\mathbf{a} \in \mathbb{W}_m} \{\rho({}_{\mathbf{a}}\mathbf{x}, \mathbf{y})\} \tag{2.1}$$

In order to find the constrained canonical correlation coefficient, one must solve the ordinary CCA problem for all possible subvectors ${}_{\mathbf{a}}\mathbf{x}$ with $\mathbf{y}$, and pick the largest correlation for which the regression weights fulfill the non-negativity constraints.

2.5. Algorithmic description of feature-based approach

For reasons of clarity, we resume our method:

- STEP 1: Tumor typing:
  For every voxel:
  1. Compute constrained CCA with spectral model of normal tissue

2. Compute constrained CCA with spectral model of CSF
3. Compute constrained CCA with spectral model of first tumor type
4. ...
5. Compute constrained CCA with spectral model of last tumor type

and type the voxel according to the highest canonical correlation coefficient.
The highest tumor grade of all voxels is detected and used in step 2.

- STEP 2: Segmentation:
For every voxel:

1. Compute constrained CCA with spectral model of normal tissue
2. Compute constrained CCA with spectral model of CSF
3. Compute constrained CCA with spectral model of detected tumor type in step 1
4. Compute constrained CCA with spectral model of corresponding mixed tissue

and type the voxel according to the highest canonical correlation coefficient.
This gives the segmentation.

3. MATERIALS

3.1. Data acquisition

In this study, data from 24 patients with a brain tumor and from 4 volunteers are used. This study has been approved by the ethical committee of the University Medical Center Nijmegen, and from all patients written informed consent was obtained. These data were obtained within the EU project INTERPRET *(1)*. Each patient's tumor was diagnosed by consensus on a histopathological study. The diagnosis was done according to the rules of the World Health Organization (WHO). 10 patients had a glial brain tumor of grade II, 5 of grade III and 7 of grade IV (glioblastoma) and 3 patients were diagnosed with a meningioma tumor. The MR data was acquired with a 1.5 T Siemens Vision whole body scanner, using a CP-head coil. For every patient first 4 MR images were acquired: T_1 weighted (TE/TR=15/644ms), T_2 weighted (TE/TR=16/3100ms), proton density weighted (TE/TR=98/3100ms) and a Gadolinium enhanced T_1 image (15 ml 0.5 M Gd-DTPA). Also both water suppressed and unsuppressed proton MR Spectroscopic Images were acquired. This MRSI data set was acquired using a 2D STEAM pulse sequence with the STEAM box positioned in a transversal plane through the brain showing the largest tumor in the Gd-image. MRSI parameters were: 16x16x1024 samples, TR/TE/TM=2000 or 2500/20/30 ms, slice thickness = 12.5 or 15 mm, FOV = 200 mm, spectral width = 1000 Hz and NS=2. Eddy current correction was performed *(39, 40)*, followed by water removal with HLSVD-PRO *(37)*, and finally a simple baseline correction was done by filtering the time signal with a highpass filter with a filterwidth of 5 ms, followed by the subtraction of the residual from the original time domain signal. Zero order phase was already corrected during eddy current correction. Manually all first order phases were adjusted. Finally, all spectra were normalised with respect to the water signal *(22)*.

3.2. Construction of simulated MRS images

From the *in vivo* data set, a large database of representative spectra for the different tumor types, normal tissue and CSF was created for simulating purposes. This database was divided in two parts. From each tissue type, 25 spectra were used to construct the spectral model, shown in figure 4. Before constructing the spectral model, the individual spectra were normalised as described in appendix A. As can be seen, the spectra show that the different tissue types are characterised by different contributions of the metabolites of interest. The other spectra were used to simulate 10x10 MRS images for each tissue type as shown in figure 5. The mixed spectra for all tumor types in these MRS images were artificially generated by averaging out a normal and a tumor spectrum.

Three types of simulated MRS images were created in order to evaluate the performance of CCA: simulations were done with spectra, simulations were done with a set of 10 quantified metabolite concentrations and simulations were done with a set of 14 features (10 metabolite concentration variables and 4 image variables). In the spectra case, for each tissue type, the database was randomly split up 5 times in order to obtain different model spectra and simulated MRS images. As there were four different tissue types in the database (grade II, grade III, glioblastoma and meningioma), the CCA-method was evaluated on 20 images with different spatial models. As a comparison also the result of ordinary correlation is computed.
For the case with 10 metabolite tissue levels, the whole database was quantified. Using the same partitioning of the database as in the spectra case, the 20 corresponding grids of sets of metabolite levels were created.
For the third series of simulations, the image variables were added to the quantified metabolite levels. With this set of features, again the corresponding grids were constructed.

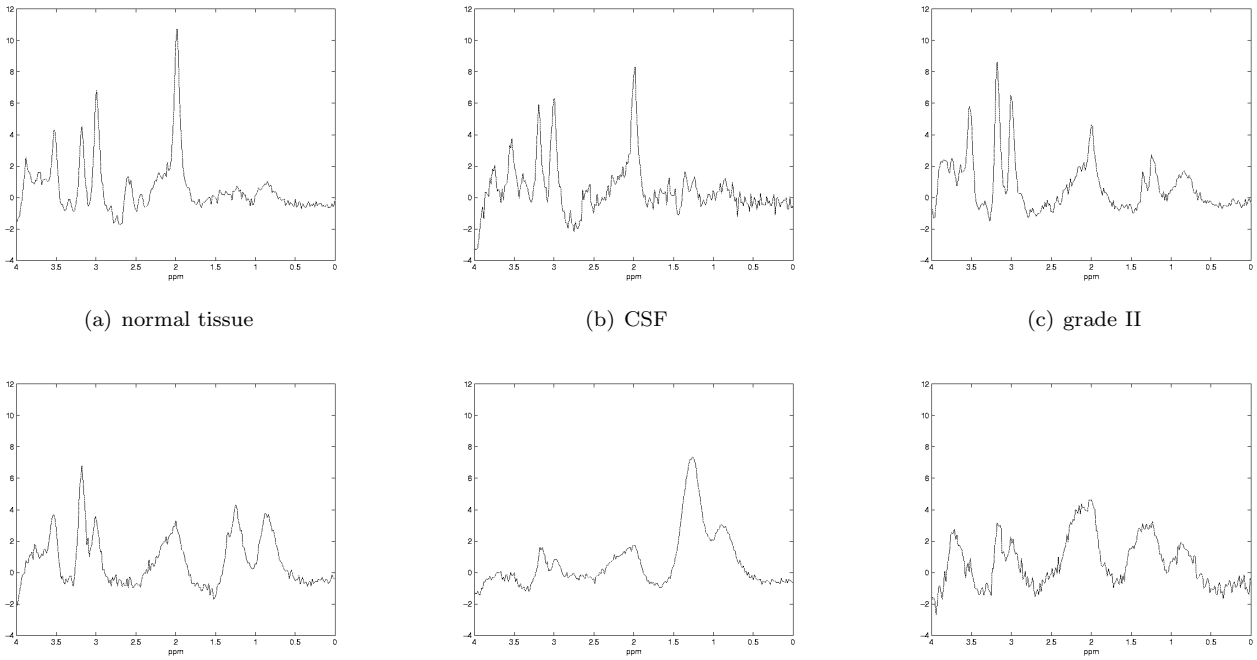

(a) normal tissue (b) CSF (c) grade II

(d) grade III (e) glioblastoma (f) meningioma

FIG. 4: Real part of the mean, $\mathbf{y}_1$, in the spectral model for the different tissue types, present in this study

4. RESULTS AND DISCUSSION

4.1. Simulations

Figure 6 demonstrates the necessity of our two-steps method. The left figure shows the result on a simulated MRSI example of grade III when all the possible spectral models are used. The region with normal tissue (1) and the region with tumor tissue of grade III (4) are detected. In the transition region, voxels are assigned to grade II (3), mixed tissue of grade II (7), mixed tissue of grade III (8) and mixed tissue of meningioma (10). We simulated the image with only grade III spectra and spectra of mixed grade III. It is clear a lot of voxels are assigned to wrong tissue classes. In figure 6b, the first step of our two-steps method is applied: only spectral models of normal and pure tumor are used. A region with normal tissue (1) and a region with grade III tumor (4) are segmented. In addition, two voxels are assigned to grade II (3). As clinicians type the tumor with respect to the most malignant tissue present, the detected tumor type is convincingly grade III. In our second step (figure 6c), the MRS image is analysed with spectral models of normal tissue (1), tumor (4) and mixed (8) tissue of grade III. Three homogenous regions are segmented. Compared to figure 6a, this result is certainly more correct and more easy to interpret.

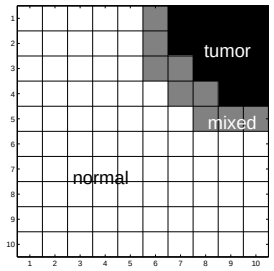

FIG. 5: Artificially created MRS image, partitioned into normal, mixed and tumor tissue. This partition was used for all the simulated MRS images

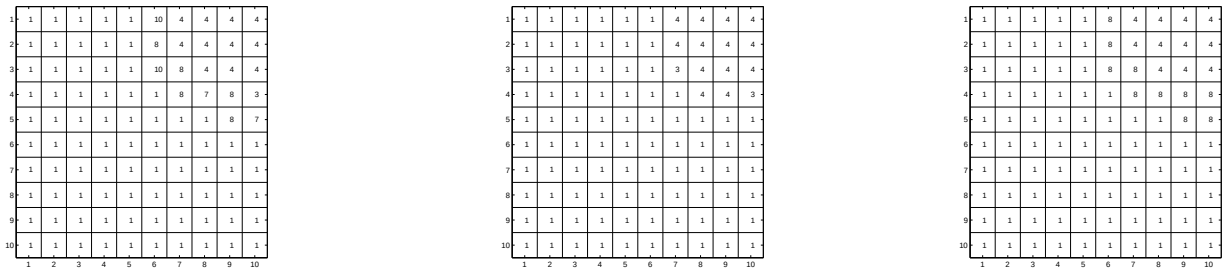

(a) (b) (c)

FIG. 6: The result of CCA on spectra with spatial 'star' model on a simulated MRSI example with a grade III tumor, (a) when all the spectral models are used, (b) step one for tumor labeling: only spectral models of normal and tumor tissue are used, (c) step two for tissue segmentation: only spectral models of normal tissue, the detected tumor and corresponding mixed tissue are used. Explanation of numbers: 1 normal; 2 CSF; 3 grade II; 4 grade III; 5 glioblastoma; 6 meningioma; 7 mixed grade II; 8 mixed grade III; 9 mixed glioblastoma; 10 mixed meningioma

On all the simulated MRS images, CCA found in the first step the correct tumor type. This is explained by the fact that the simulations are constructed with a database containing only carefully selected spectra! In the rest of this section, we only discuss the segmentation accuracy.
Before discussing more general results, it is useful to have a closer look at the segmentation result on one simulated MRS image. Figure 7 compares the result of ordinary correlation (a-b) with the result of CCA (c-d) using the spatial 'star' model on a grade II tumor. The red, green and blue regions contain respectively the detected tumor, mixed and normal tissue. The example clearly shows the advantage of using spatial information: ordinary correlation doesn't segment homogeneous regions, but assigns a lot of isolated voxels to the wrong tissue type. Especially the distinction between tumor tissue and mixed tissue seems difficult. The CCA-based method detects correctly the tumor region, surrounded by a band of mixed tissue. This results in a segmentation accuracy of 98% for CCA. It is observed that most of the misclassified voxels are corner voxels. This is logical, because corner voxels are surrounded by less voxels of the same tissue type. On figure 7, we cannot see differences between the CCA-method on spectra and features. Both perform in this case similarly. It is however interesting to note that misclassified voxels in the spectra case not necessarily correspond to misclassified voxels in the feature case.
A question that can arise is how reliable the result is. CCA gives a canonical correlation coefficient that is a measure of the similarity between the voxel under investigation and a model spectrum. This canonical correlation coefficient is for all voxels in the spectra case between 0.91 and 0.98, and in the features case between 0.95 and 0.999. This is much higher than the correlation coefficients of ordinary correlation (0.7-0.8). However no direct measure of reliability can be derived from the canonical correlation coefficient itself. The canonical correlation coefficient will rather reflect the amount of noise/artefacts in the data. A measure of reliability that can be introduced is the smallest difference between two canonical correlation coefficients, shown in figure 7e-f. When two canonical correlation coefficients are very close to each other, the probability of missclassification is much higher than in the case when one canonical correlation coefficient is higher than the other one. Figure 7e nicely reflects this idea: in the region of the mixed tissue, the difference is smallest compared to the other regions, because the correlation with all three tissue types can be made high. However in the feature case, figure 7f doesn't add any further information.

To compare the different CCA approaches in a more general way, the segmentation accuracy of the 20 segmented images is obtained by simply counting the number of correctly classified voxels. The average value is given in table 1. The results of the CCA method are compared when different spatial models are considered. The result of ordinary correlation is added as reference value. The columns of the table correspond to three kinds of input vectors: using the MR spectra, using the quantified metabolite levels or using the features.
The lower performance of segmentation accuracy of the ordinary correlation analysis compared to CCA using a 'star' model is confirmed in Table1. It can also be seen that the chosen spatial model is not crucial for the CCA-method. Most CCA variants yield a very reliable segmentation, certainly more reliable than ordinary correlation. Only the '3x3' model doesn't seem to nicely segment the MRS image. This is probably due to overfitting. $\mathbf{X}$ contains too many basis functions, so that the spanned subspace is too large. By limiting the number of considered voxels or by averaging out voxels, the problem of overfitting will be re-

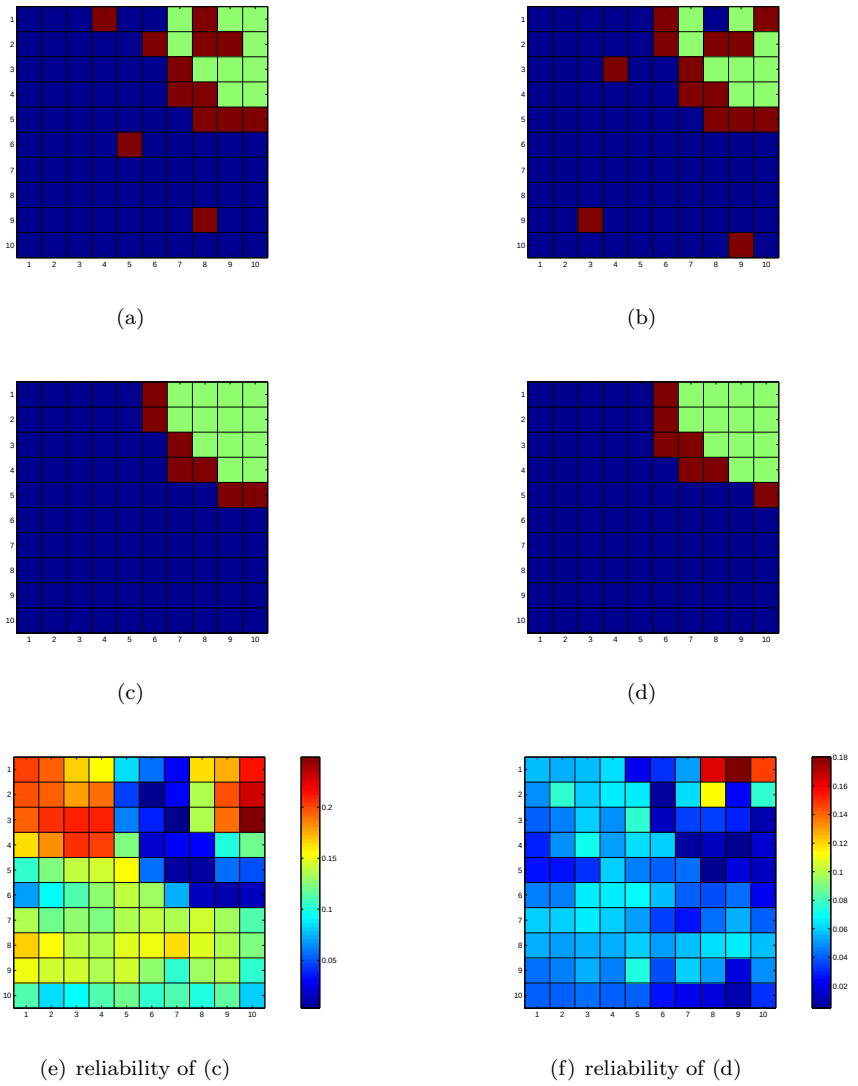

(a) (b) (c) (d) (e) reliability of (c) (f) reliability of (d)

FIG. 7: The result of (a) ordinary correlation on spectra, (b) ordinary correlation on features, (c) CCA on spectra, (d) CCA on features. (e) and (f) show the smallest difference between two canonical correlation coefficients when CCA is computed on respectively spectra and features

duced.

When the different input strategies are compared, it is clearly seen that quantifying the spectra before applying CCA reduces the segmentation accuracy. This approach should never been used, as the quantification step can introduce errors. However, quantifying the spectra makes sense when image information is added. The values displayed in the third column are higher than the values in the second column, which shows that adding image information really improves the segmentation result. The accuracy with feature sets of 14 variables is slightly higher than the accuracy of the spectra case. However, the differences are very small. Keeping in mind that we only work with 20 carefully constructed simulated examples, we can state that both approaches perform similarly in terms of accuracy.

4.2. *In vivo*

Also several *in vivo* MRS images were analysed. The CCA-results on 4 patients are discussed below. We focus in this part on differences between the two valuable approaches, namely CCA on spectra and CCA on feature sets of 14 variables. All the results are obtained with a spatial 'star' model. Care was taken that the model spectrum was constructed with 25 spectra of other patients. So independency is guaranteed. The colors of the segments in figures 8 to 11 have a specific meaning. As the used tissue types

	spectra	metabolite levels	metabolite levels + image vars
symm3x3	97.5	96.7	98.1
symm3x3 without corners	95.8	96.4	96.1
3x3	95.5	93.2	95.2
3x3 without corners	97.8	94.8	98
star	97.3	95	98.2
ordinary correlation	91	93.7	95.5

TABLE 1: The segmentation accuracy of the segmented image by CCA methods with different spatial models and crosscorrelation. The displayed value is the mean value of the results on 20 artificially generated MRS images with different tumor types. Values in %.

differ in the tumor typing and segmentation steps, it is not possible to use in both steps the same color legend. After the tumor typing step, dark blue is used for normal tissue, light blue for CSF, green for grade II, yellow for grade III, orange for glioblastoma and red for meningioma. After the segmentation step, blue represent normal tissue, green mixed tissue, orange the detected tumor tissue and red is used for CSF.

Figure 8 shows the result of CCA on features for a patient with a glioblastoma tumor after the first and the second step. In the first step several glioblastoma voxels are detected, but also several voxels at the boundary of the glioblastoma region are assigned to grade III. This can be expected, as pathologists type the patient with respect to the most malignant tissue present. The diagnosis of the method is correctly glioblastoma. In the second step most 'grade III voxels' in figure 8a are assigned to mixed tissue in figure 8b as the model spectra of grade III and mixed glioblastoma are very similar. It can also be seen that the segmented regions with CSF correspond nicely to the ventricles in the MR image.

In figure 9 the results with spectra and features are compared after the tumor typing step on a tumor of grade III. Although the detected tumor region is large, the CCA method on spectra (figure 9a) only detects one voxel of grade III in the first step. This tumor is probably very heterogeneous and only a very small part of the tumor will really be of grade III. For this patient, the diagnosis based on the most malignant tumor present, will still be correct (grade III) but this example illustrates the limitations of methods that improve robustness by including spatial information. When the tumor region is too small, the tumor will be hidden by the surrounding voxels. Compared to the result obtained with features (figure 9b) we can clearly state that the result of CCA on features is better, as there is more convincingly a grade III region detected (like in *(30)*). In the second step, both approaches gave similar results.

Figure 10 compares the segmentation results of both approaches on a meningioma tumor. The first step is not shown as a region with meningioma is convincingly detected by both CCA approaches. In the second step, the present meningioma tumor is nicely segmented in both figures. But it is also seen that the CCA method based on spectra segments three lines as a (homogeneous) region of mixed tissue. These lines contain normal spectra. However, the spectra in the lower part are of minor quality compared to the spectra in the upper part of the grid. This leads to misclassifications when CCA is applied to spectra. By quantifying the spectra and normalising the spectra in an appropriate way, the voxels are correctly classified by CCA on features!

Finally, figure 11 compares on the same patient the results of both approaches after step 1 and step 2. For this patient no histopathological agreement was reached. The pathologists who validated the tumor disagreed between grade II en grade III. Both CCA on spectra and CCA on features classify the large area as grade III. The result of ordinary correlation is not shown, but ordinary correlation assigned two voxels to glioblastoma tissue (grade IV). These are clearly misclassifications, that will lead to the wrong diagnosis. These misclassifications are avoided by the use of spatial information. The most interesting part of this example is however the right ventricle. CCA on spectra assigns these CSF-voxels wrongly to grade II (step 1) or mixed tissue (step 2). When features are used as input, the two ventricles are nicely segmented and correctly classified. This is certainly due to the incorporation of the image variables because in the MR images the ventricles are clearly visible. It can also be noted that in this figure and in figure 9, the segmentation boundaries differ between both approaches. However, it cannot be said which segmentation is the best, because no golden standard is available. In every case, in all the examples, the correct tumor type is detected. Also a comparison between the obtained segmentation and the high-resolution MR images shows that the boundary of mixed voxels obtained with the method makes sense. Furthermore, always homogeneous regions are segmented, which eases the interpretation for radiologists.

Finally, we have to remark that the use of this accurate method has one drawback. A reliable and representative

model spectrum has to be constructed for the present tissue types, in order to obtain a meaningful result. To construct all the spectral models, a database of carefully validated spectra has to be generated. This takes time, especially for rarely present tumor types. Constructing a spectral model is even 'impossible' when there are 'unexpected' tissue types in a new MRSI dataset. In this study, 'unexpected' tissue types are e.g. edema, necrosis, ... During the on-going European eTumour project *(2)*, a large database of all possibly expected tissue types (adults & children) is being constructed. With this database, optimal spectral models can be generated. We expect that our CCA-based method with these spectral models will in the future reliably assign MRSI voxels to the correct histopathological class.

5. CONCLUSION

CCA is a technique that quantifies the relationship between two multivariate vectors. In *(21)* CCA was succesfully applied to segment long echo-time prostate MRSI. In this paper, a CCA-based method is introduced to translate short echo-time brain MRS images into easy-to-understand nosologic images. In order to distinguish in a reliable way between different brain tumor types, a two-steps method is presented. The first step is a tumor typing step and in the second step the heterogeneity of the detected tumor is shown. In addition, we introduce a CCA-based method on feature sets. This feature sets integrate information of MRSI and MRI. We also show that the CCA-based method on such feature sets outperforms the CCA-based method on the whole spectra in *in vivo* cases.

6. APPENDIX A

On the standardization of the model spectra

Although the spectra were already normalised with respect to the water peak, the segmentation could be improved by standardizing these water-normalised spectra, i.e., subtracting the mean (centering) and dividing by the standard deviation (scaling). The segmentation based on classifying voxels according to the highest canonical correlation coefficient improved not much by this extra normalisation step. However, the smallest difference between two canonical correlation coefficients became larger (figure 12). This shows that the discriminating power of the method becomes bigger when the spectra are standardized.

Also in the feature case, the sets of features were also standardized by subtracting the mean and dividing by the standard deviation.

ACKNOWLEDGMENTS

Research funded by a PhD grant of the Institute for the Promotion of Innovation through Science and Technology in Flanders (IWT-Vlaanderen).

Research supported by **Research Council KUL**: GOA-AMBioRICS, CoE EF/05/006 Optimization in Engineering, several PhD/postdoc & fellow grants; **Flemish Government**: FWO: PhD/postdoc grants, projects, G.0407.02 (support vector machines), G.0360.05 (EEG, Epileptic), G.0519.06 (Noninvasive brain oxygenation), G.0321.06 (Tensors/Spectral Analysis), research communities (ICCoS, ANMMM);IWT: PhD Grants; **Belgian Federal Science Policy Office** IUAP P5/22 ('Dynamical Systems and Control: Computation, Identification and Modelling'); **EU**:INTERPRET(FP5), BIOPATTERN (FP6-2002-IST 508803), ETUMOUR (FP6-2002-LIFESCIHEALTH 503094), Healthagents (IST200427214).

REFERENCES

(1) http://carbon.uab.es/INTERPRET/

(2) http://www.etumour.net/

(3) S. Das and P. Sen, Restricted Canonical Correlations, Linear Algebra and its Applications, 210, 29-47 (1994)

(4) T. Laudadio, M.C. Martinez-Bisbal, B. Celda and S. Van Huffel, Fast nosological imaging of 2DTSI brain data using Canonical Correlation Analysis, Internal Report 05-250, ESAT-SISTA, K.U.Leuven (Leuven, Belgium) (2005).

(5) S. Mierisova, A. van den Boogaart, I. Tkae, P. Van Hecke, L. Vanhamme, V. Mlynarik and T. Liptaj, AMARES: a new Approach for Quantitation of Short Echo Time in vivo ^{1}H Spectra of Rat Brain, NMR in Biomed., 11, 32-39 (1998)

(6) M. Omladic and V. Omladic, More on restricted canonical correlations, Linear Algebra and its Applications, 321, 285-293 (2000)

(7) M. Bernstein, A.G. Parrent, Complications of CT-guided stereotactic biopsy of intra-axial brain lesions, J. Neurosurg., 81, 165-168 (1994)

(8) S.J. Nelson, Minireview: Multivoxel Magnetic Resonance Spectroscopy of Brain Tumors, Molec. Cancer Therap., 2, 497-507 (2003)

(9) M. Castillo, J.K. Smith, L. Kwock, Correlation of myo-inositol levels and grading of cerebral astrocytomas, Am. J. Neuroradiol., 21, 1645-1649 (2000)

(10) S.J. Barton, F.A. Howe, A.M. Romlins, S.A. Cudlip, J.K. Nicholson, B.A. Bell, J.R. Griffiths, Comparison of ^{1}H MRS of human brain tumours with ^{1}H HR-MAS spectroscopy of intact biopsy samples in vitro,

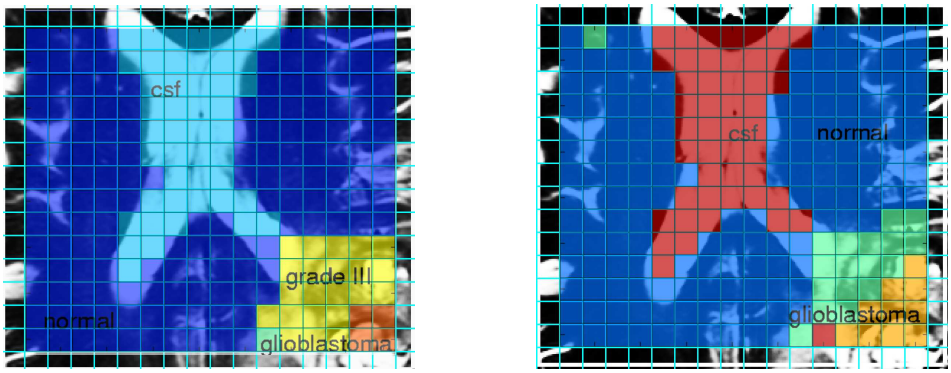

(a) tumor typing step (b) segmentation step

FIG. 8: The result of CCA on features with spatial 'star' model (a) after the tumor typing step and (b) after the segmentation step

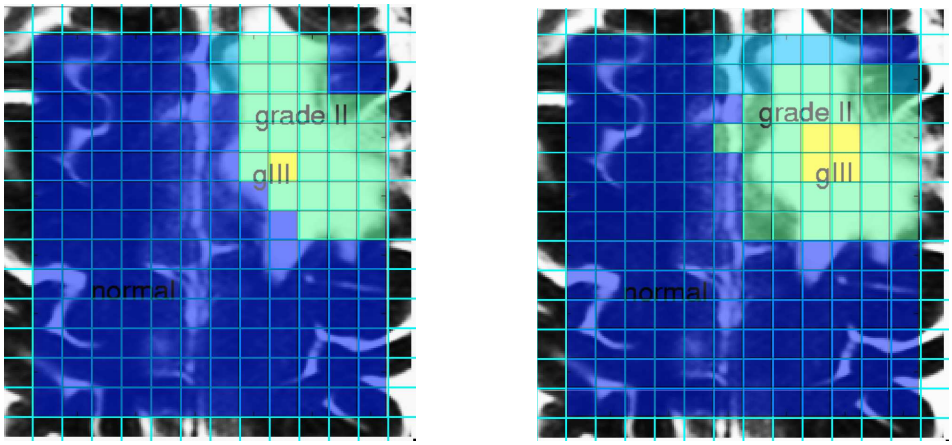

(a) CCA on spectra (b) CCA on features

FIG. 9: The result of CCA with spatial 'star' model after the tumor typing step (a) applied on spectra and (b) applied on features

Magn. Res. Mat. in Phys., Biol. and Med., 8, 121-128 (1999)

(11) A.R. Tate, C. Majós, A. Moreno, F.A. Howe, J.R. Griffiths, C. Arus, Automated classification of short echo time spectra in in vivo ^{1} brain spectra: a multicenter study, Magn. Res. Med., 49, 29-36 (2003)

(12) M.C. Preul, Z. Caramanos, R. Leblanc, J.G. Villemure, D.L. Arnold, Using pattern analysis of *in vivo* proton MRSI data to improve the diagnosis and surgical management of patients with brain tumors, NMR in Biomed., 11, 192-200 (1998)

(13) H. Hotelling, Relations between two sets of variates, Biometrika, 28, 321-371 (1936)

(14) G. Fan, B. Sun, Z. Wu, Q. Guo, Y. Guo, In vivo single-voxel proton MR spectroscopy in the differentiation of high-grade gliomas and solitary metastases, Clin. Radiol., 59, 77-85 (2004)

(15) C. Majos, M. Julia-Sape, J. Alonso, M. Serrallonga, C. Aguilera, J.J. Acebes, C. Arus, J. Gili, Brain Tumor Classification by Proton MR Spectroscopy: Comparison of Diagnostic Accuracy at Short and Long TE, Am. J. Neuroradiol., 25, 1696-1704 (2004)

(16) K.S. Opstad, M.M. Murphy, P.R. Wilkins, B.A. Bell, J.R. Griffiths, F.A. Howe, Differentiation of metastases from high-grade gliomas using short echo time ^{1} H spectroscopy, Magn. Res. Imag., 20, 187-192 (2004)

(17) D.P. Auer, Ch. Gössl, T. Schirmer, M. Czisch, Improved lipid analysis of ^{1}-MR spectra in the presence of mobile lipids, Magn. Res. Med., 46, 615-618 (2001)

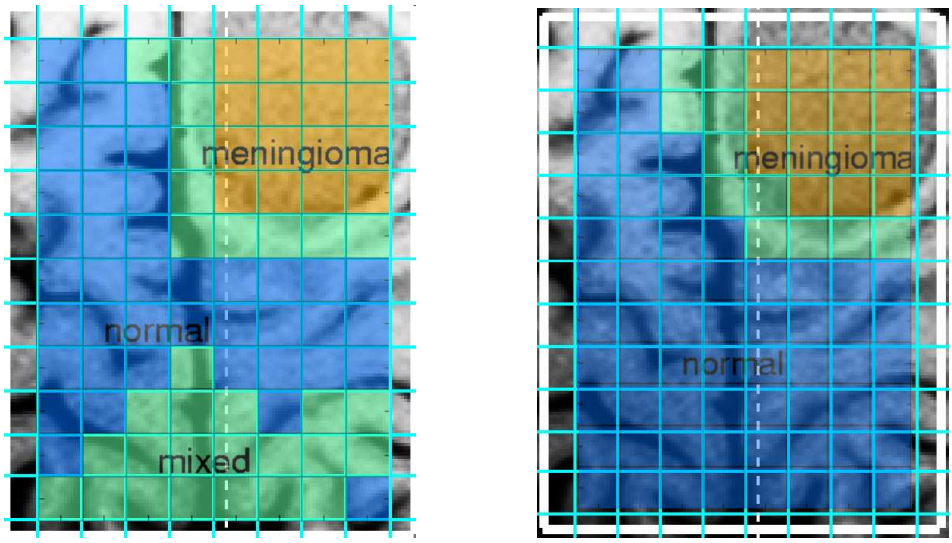

(a) CCA on spectra (b) CCA on features

FIG. 10: The result of CCA with spatial 'star' model after the tumor typing step (a) applied on spectra and (b) applied on features for a patient with a meningioma tumor

(18) J. Lindon, E. Holmes, J. Nicholson, Pattern recognition methods and applications in biomedical magnetic resonance, Prog. Nucl. Magn. Res. Spectr., 39, 1-40 (2001)

(19) R. Duda, P. Hart, D. Stork, Pattern classification, 2nd edition John Wiley & Sons (2001)

(20) G. Hagberg, A.P. Burlina, I. Mader, W. Roser, E.W. Radue, J. Seelig, In vivo proton MR spectroscopy of human gliomas: definition of metabolic coordinates for multi-dimensional classification, Magn. Res. Med., 34, 242-252 (1995)

(21) T. Laudadio, P. Pels, L. De Lathauwer, P. Van Hecke, S. Van Huffel, Tissue segmentation and classification of MRSI data using Canonical Correlation Analysis, Magn. Res. Med., 54, 1280-1284 (2005)

(22) Z. Tong, T. Yamaki, K. Harada, K. Houkin, In vivo quantification of metabolites in normal brain and brain tumors by proton MR spectroscopy using water as an internal standard, Magn. Res. Imag., 22, 1017-1024 (2004)

(23) L. Vanhamme, A. van den Boogaart, S. Van Huffel, Improved Method for accurate and efficient quantification of MRS data with use of prior knowledge, J. Magn. Res., 129, 35-43 (1997)

(24) U. Seeger, U. Klose, I. Mader, W. Grodd, T. Nägele, Parameterized Evaluation of Macromolecules and Lipids in Proton MR Spectroscopy of Brain Diseases, Magn. Res. Med., 49, 19-28 (2003)

(25) B.J. Soher, K. Young, A.A. Maudsley, Representation of strong baseline contributions in ^{1}H MR spectra, Magn. Res. Med., 45, 966-972 (2001)

(26) K. Young, B.J. Soher, A.A. Maudsley, Automated spectral analysis II: application of wavelet shrinkage for characterization of non-parametric signals, Magn. Res. Med., 40, 816-821 (1998)

(27) L. Hofmann, J. Slotboom, C. Boesch, R. Kreis, Characterization of the Macromolecule Baseline in Localized ^{1}H-MR Spectra of Human Brain, Magn. Res. Med., 46, 855-863 (2001)

(28) K.L. Behar, D.L. Rothman, D.D. Spencer, O.A. Petroff, Analysis of macromolecule resonances in 1H-MR spectra spectra of human brain, Magn. Res. Med., 32, 294-302 (1994)

(29) O. Friman, Adaptive Analysis of Functional MRI Data, PhD thesis, Linköping University, Sweden, 2003

(30) A. Simonetti, W. Melsen, M. van der Graaf, G. Postma, A. Heerschap, L. Buydens, A chemometric approach for brain tumor classsification using magnetic resonance imaging and spectroscopy, Anal. Chem., 75, 5352-5361 (2003)

(31) J. Slotboom, C. Boesch, R. Kreis, Versatile frequency domain fitting using time domain models and prior knowledge, Magn. Res. Med., 39, 899-911 (1998)

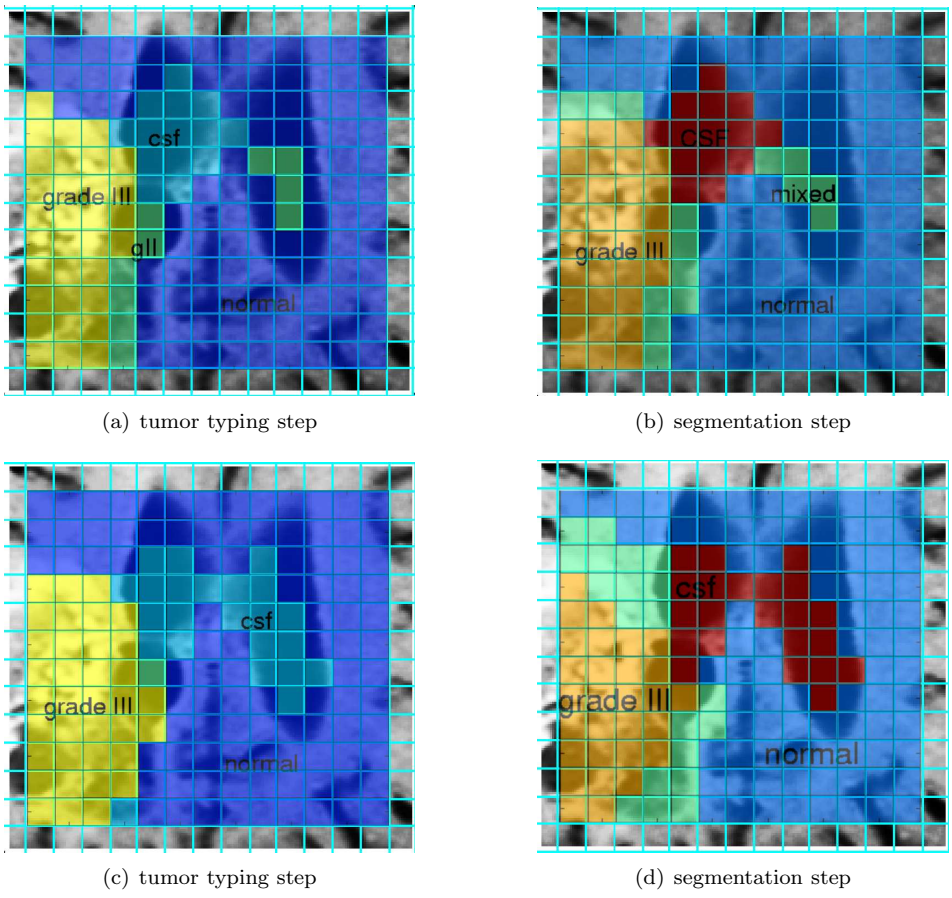

(a) tumor typing step (b) segmentation step

(c) tumor typing step (d) segmentation step

FIG. 11: The result of CCA on spectra using spatial 'star' model (a) after the tumor typing step and (b) after the segmentation step and the result of features in (c) and (d)

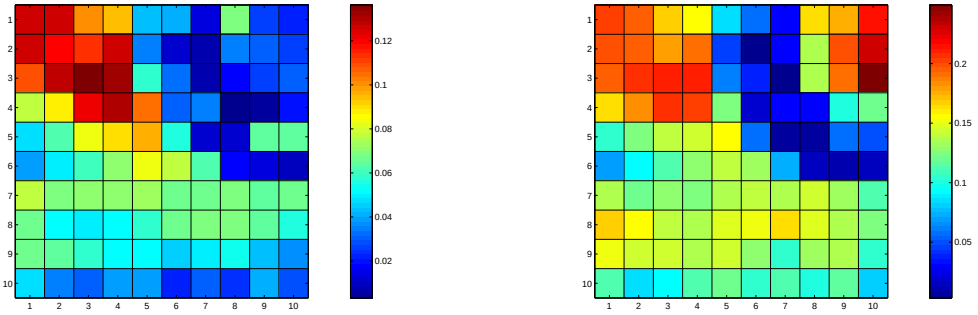

(a) without standardization (b) with standardization

FIG. 12: The smallest difference between two canonical correlation coefficients is shown when (a) the spectra are only normalised with respect to the height of the waterpeak and (b) when the spectra are also standardized. The figure shows that the discriminating power nearly doubles by normalising the individual spectra

(32) B.J. Soher, K. Young, A.A. Maudsley, Automated spectral analysis III: application to in vivo proton MR spectroscopy, Magn. Res. Med., 40, 822-831 (1998)

(33) H. Ratiney, Y. Coenradie, S. Cavassila, D. van Ormondt, D. Graveron-Demilly, Time domain quantitation of ^{1}H short echo-time signals: background accomodation, MAGMA, 16, 284-296 (2004)

(34) A. Devos, A.W. Simonetti, M. van der Graaf, L. Lukas, J.A. Suykens, L. Vanhamme, L.M Buydens, A. Heerschap, S. Van Huffel, The use of multivariate MR imaging intensities versus metabolic data from MR spectroscopic imaging for brain tumour classification, J. Magn. Res., 173, 218-282 (2005)

(35) B. Wilken, P. Dechent, Herms J, Maxton C, Markakis E, Hanefeld F, Frahm J, Quantitative proton magnetic resonance spectroscopy of focal brain lesions, J. Pediatr. Neurol., 23, 22-31 (2000)

(36) B. Mirkin, Clustering for data mining, Chapmann & Hall/CRC, Florida, USA (2005)

(37) T. Laudadio, N. Mastronardi, L. Vanhamme, P. Van Hecke and S. Van Huffel, *Improved Lanczos algorithms for blackbox MRS data quantitation,* J. Magn. Res., Vol. 157, pp. 292-297, 2002.

(38) F. Szabo De Edelenyi, C. Rubin, F. Estve, G. Sylvie, M. Dcorps, V. Lefournier, J-F. Le Bas, C. Rmy, A new approach for analyzing proton magnetic resonance spectroscopic images of brain tumors: nosologic images, Nat. Med., 6, 1287-1298 (2000)

(39) A.W. Simonetti, W.J. Melssen, M. van der Graaf, A. Heerschap, L.M. Buydens, Automated correction of unwanted phase jumps in reference signals which corrupt MRSI spectra after Eddy current correction, J. Magn. Res., 159, 151-157 (2002)

(40) U. Klose, In vivo proton spectroscopy in presence of eddy currents, Magn. Res. Med., 14, 26-30 (1990)

(41) S. W. Provencher, Estimation of metabolite concentrations from localized *in vivo* proton NMR spectra, Magn. Res. Med., 30, 672-679 (1993)

(42) A.W. Simonetti, J-B. Poullet, D.M. Sima, B. De Neuter, L. Vanhamme, Ph. Lemmerling, S. Van Huffel, An open source short echo time MR quantitation software solution: AQSES, Internal Report 05-168, ESAT-SISTA, K.U.Leuven (Leuven, Belgium), 2005.